Long-Cycle-Life Calcium Battery with a High-Capacity Conversion Cathode Enabled by a Ca^{2+}/Li^{+} Hybrid Electrolyte

Zhen Meng,* Adam Reupert, Yushu Tang, Zhenyou Li, Guruprakash Karkera, Liping Wang, Ananyo Roy, Thomas Diemant, Maximilian Fichtner, and Zhirong Zhao-Karger*

ABSTRACT: Calcium (Ca) batteries represent an attractive option for electrochemical energy storage due to physicochemical and economic reasons. The standard reduction potential of Ca (−2.87 V) is close to Li and promises a wide voltage window for Ca full batteries, while the high abundance of Ca in the earth's crust implicates low material costs. However, the development of Ca batteries is currently hindered by technical issues such as the lack of compatible electrolytes for reversible Ca^{2+} plating/stripping and high-capacity cathodes with fast kinetics. Herein, we employed FeS_2 as a conversion cathode material and combined it with a Li^{+}/Ca^{2+} hybrid electrolyte for Ca batteries. We demonstrate that Li^{+} ions ensured reversible Ca^{2+} plating/stripping on the Ca metal anode with a small overpotential. At the same time, they enable the conversion of FeS_2, offering high discharge capacity. As a result, the Ca/FeS_2 cell demonstrated an excellent long-term cycling performance with a high discharge capacity of 303 mAh g^{-1} over 200 cycles. Even though the practical application of such an approach is questionable due to the high quantity of electrolytes, we believe that our scientific findings still provide new directions for studying Ca batteries with long-term cycling.

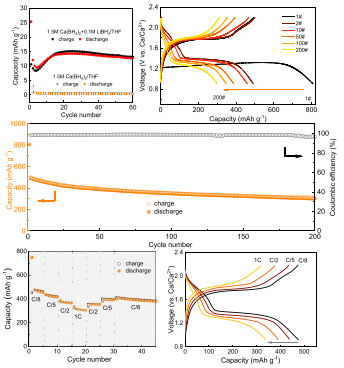

KEYWORDS: *FeS_2 cathode, Ca anode, hybrid electrolyte, long-term cycling, Ca battery*

1. INTRODUCTION

Multivalent-ion batteries have received increasing attention in recent years. In this context, calcium ion (Ca^{2+} ion)-based battery chemistry is one of the most promising candidates among these emerging technologies. The Ca/Ca^{2+} couple could theoretically deliver a capacity of 1340 mAh g^{-1} with a low standard reduction potential of −2.87 V, which is only 0.17 V difference from Li. Furthermore, Ca is the fifth most abundant element in the earth's crust and is environmentally benign. Nevertheless, reversible Ca plating/stripping is still challenging due to the lack of compatible electrolytes. Recently reported fluoride-based electrolytes exhibit reversible Ca plating/stripping and high anodic stability. However, the CaF_2 formation on the surface lowers the Coulombic efficiency and impedes Ca^{2+} migration.[1−3] The electrolyte based on $Ca(BH_4)_2$ exhibited better Ca plating/stripping performance due to the absence of a passivation layer on the Ca surface. Although the oxidation stability is <3 V versus Ca/Ca^{2+}, it is suitable to evaluate the cathode materials in this voltage window. Another hurdle toward rechargeable Ca batteries is the lack of proper cathode host materials. Different from the extensive success of intercalation cathodes in Li-ion batteries experimentally and theoretically, Ca-ion intercalation is challenging as the highly charged cation can induce polarization within the host environment.[4] Organic materials and conversion cathodes based on sulfur have been investigated for Ca batteries very recently,[5−7] which could circumvent the intrinsic drawbacks of intercalation chemistry and potentially offer high capacities.

To explore new cathode candidates and enhance the electrochemical performance of the multivalent batteries, the dual-salt electrolyte concept has been proposed, where Li^{+} or Na^{+} coexists with multivalent ions (Ca^{2+} and Mg^{2+}) in the electrolyte. These coexisting monovalent metal ions could primarily promote the redox reaction at the Ca or Mg anode by either being involved in the solid electrolyte interphase (SEI) formation[8,9] or manipulating the solvation of multivalent ions.[10] The usage of dual-salt electrolytes also provides wide options for cathodes. For instance, dual-salt electrolytes have been used for hybrid or dual-ion battery systems by combining a Li^{+}-ion intercalation cathode with a multivalent metal anode.[11−16] Li^{+} ions could also mediate a polysulfide reaction, thus boosting the Mg−S and Ca−S battery performance.[17,18] Other conversion cathodes, such as FeS_2 and FeS, have been investigated with the $Mg(BH_4)_2/LiBH_4$/tetrahydrofuran (THF) electrolyte,[19] which combines the virtues of smooth

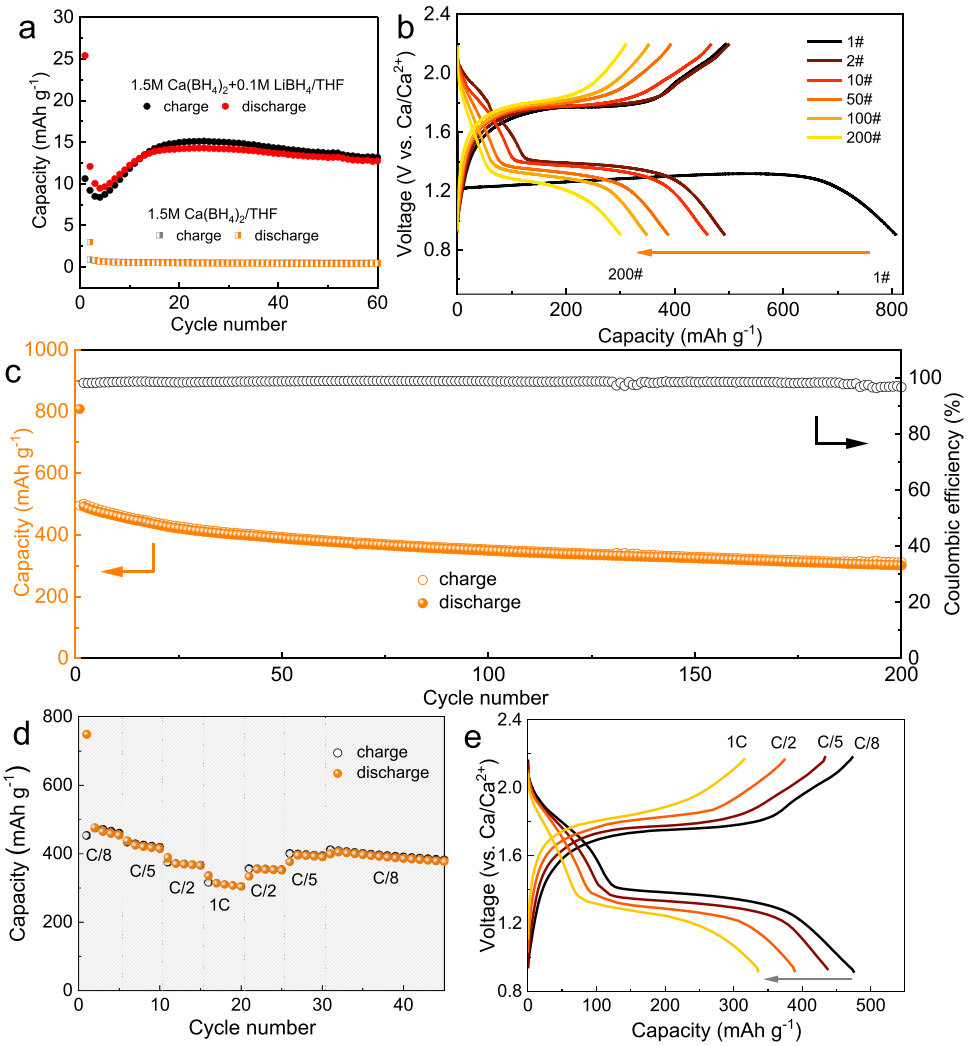

Figure 1. Electrochemical performance of the FeS_2/Ca cell with (a) 1.5 M $Ca(BH_4)_2$/THF, 1.5 M $Ca(BH_4)_2$ + 0.1 M $LiBH_4$/THF electrolytes at C/8, (b–e) 0.5 M $Ca(BH_4)_2$ + 1.5 M $LiBH_4$/THF electrolyte: (b) voltage profile at C/8, (c) long-term cycling at C/8, (d) rate performance, and (e) voltage profile at different C-rates.

Mg plating/stripping and kinetically favorable Li-driven conversion of FeS_x.

Herein, an FeS_2-based conversion cathode was employed for Ca batteries. FeS_2 has been investigated as a Li and Na storage material.[20−23] Based on the redox reactions of Fe^{2+}/Fe^0 and S_2^{2-}/S^{2-}, it offers a high theoretical capacity of 894 mAh g^{-1}. However, our initial experiments indicated the absence of reversible conversion of FeS_2 in the Ca system with $Ca[B(hfip)_4]_2$/DME or $Ca(BH_4)_2$/THF single-salt electrolytes. In contrast, adding Li^+ ions by using the $Ca(BH_4)_2$/$LiBH_4$/THF electrolyte could significantly boost the performance. The results proved that the Li^+ ion played a crucial role in enabling the reversible cycling performance of the cathode. On the anode side, $LiBH_4$ may facilitate reversible Ca plating/stripping over long-term cycling by lowering the Ca^{2+} ion desolvation energy.[10] As a result, Ca batteries with long cycle life and stable capacity retention were demonstrated. It should be noted that a high electrolyte/cathode ratio is necessary to ensure the conversion (>22.5 μL/mg; see the Supporting Information, electrolyte-to-cathode ratio calculation), which will decrease the energy density of the cell. However, the positive effect of Li^+ on both the anode and cathode sides still provides a new direction for us to achieve a Ca battery with long cycle life.

2. EXPERIMENTAL SECTION

2.1. Preparation of FeS_2. FeS_2 was synthesized according to previous literature.[24] Briefly, Fe_3O_4 and sulfur powder were mixed in a weight ratio of 1:1.5 and sealed into a quartz tube under vacuum, which was subsequently heated in a furnace with a ramp of 2 °C min^{-1} at 600 °C and kept at this temperature for 2 h. After cooling down to room temperature, the powder was washed with CS_2 several times to remove the residual sulfur. The successful preparation of FeS_2 with a cubic structure was confirmed by X-ray diffraction (XRD) measurements (Figure S1). Furthermore, SEM images (Figure S2) showed that the particle size varied from 100 nm to micron.

2.2. Preparation of Electrolytes. THF was dried with 3 Å molecular sieves before use. $Ca(BH_4)_2$•2THF and $LiBH_4$ were used as received. Three electrolyte mixtures were prepared (1.5 M $Ca(BH_4)_2$/THF, 1.5 M $Ca(BH_4)_2$ + 0.1 M $LiBH_4$/THF, and 1.5 M $LiBH_4$ + 0.5 M $Ca(BH_4)_2$/THF) by adding appropriate amounts of $Ca(BH_4)_2$•2THF and $LiBH_4$ to THF (viz., 321 mg of $Ca(BH_4)_2$•2THF, 321 mg of $Ca(BH_4)_2$•2THF + 2.2 mg of $LiBH_4$, and 107 mg of $Ca(BH_4)_2$•2THF + 33 mg of $LiBH_4$ into 1 mL of THF, respectively). After stirring overnight and waiting for 1 day, the supernatant was used as the electrolyte. It should be noted that the concentration values (1.5, 0.1, and 0.5 M) here are just used to

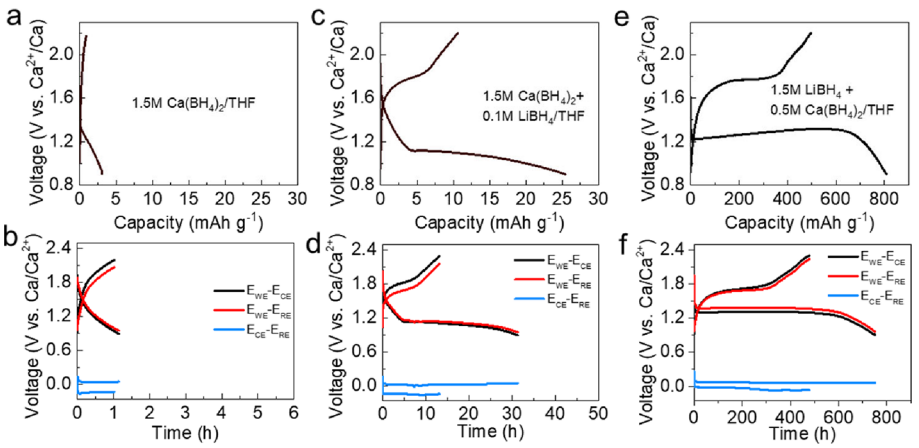

Figure 2. Voltage profiles of two-electrode (a, c, e) and three-electrode (b, d, f) FeS_2−Ca cells: (a, b) 1.5 M $Ca(BH_4)_2$/THF, (c, d) 1.5 M $Ca(BH_4)_2$ + 0.1 M $LiBH_4$/THF, and (e, f) 0.5 M $Ca(BH_4)_2$ + 1.5 M $LiBH_4$/THF.

distinguish the electrolytes. They are not the real molarities of electrolytes since some insoluble residue was still visible in all cases after stirring overnight, and the electrolyte volume would change once the salt is added to the solvent. The exact values for these electrolytes were 1.22 M $Ca(BH_4)_2$/THF, 1.22 M $Ca(BH_4)_2$ + 0.082 M $LiBH_4$/THF, and 1.33 M $LiBH_4$ + 0.44 M $Ca(BH_4)_2$/THF, respectively (Supporting Information).

2.3. Electrochemical Measurement. For the FeS_2 electrodes, FeS_2, Super P, and PVDF were mixed in a weight ratio of 7:2:1 with NMP solvent. The slurry was dropped on the carbon paper, followed by drying under vacuum at 80 °C overnight. The FeS_2 loading was 1−1.5 mg cm^{-2}. For Ca electrodes, calcium shot was pressed into disks. Two pieces of glass fiber sheets (GF/C, Whatman) were used as separators for cell assembly. The electrochemical measurements of the FeS_2 electrodes were carried out with CR2032 coin cells with 80 μL of electrolyte. The electrolyte-to-cathode ratio is 113 μL/mg. Tests with symmetric cells were conducted with Swagelok cells with 60 μL of electrolyte. For the three-electrode test, a PAT-Cell (from EL-Cell) was used with 200 μL of electrolyte. The measurements were performed using a Bio-Logic VMP3 potentiostat and an Arbin battery cycling unit at room temperature.

2.4. Material Characterization. XRD measurement was carried out with a Bruker D8 ADVANCE XRD diffractometer with a Cu K_α source. A Zeiss LEO 1530 was used for scanning electron microscopy (SEM) analysis. Transmission electron microscopy (TEM) characterization was performed on a probe-corrected microscope Themis300 (Thermo Fisher Scientific) and a double aberration-corrected microscope ThemisZ (Thermo Fisher Scientific) at an acceleration voltage of 300 kV. The TEMs were equipped with a high-angle annular dark-field scanning transmission electron microscopy (HAADF-STEM) detector and a Super-X EDX detector to acquire energy-dispersive X-ray spectroscopy (EDS) maps. The TEM specimen was prepared inside the glovebox by scratching the electrode material with a lacey carbon-coated gold grid. Afterward, the grid was mounted into a Gatan 648 vacuum transfer holder, which can be used to transfer the specimen into the TEM under Ar protection. The X-ray photoelectron spectra (XPS) were acquired on a Specs XPS system with a Phoibos energy analyzer using monochromatic Al K_α radiation (1486.6 eV), a take-off angle of 45°, and pass energies of 30 and 90 eV at the analyzer for detail and survey spectra, respectively. The samples were transferred under Ar from the glovebox to the XPS system to avoid contamination. CasaXPS was used for data analysis, using Shirley-type backgrounds and Gaussian−Lorentzian peak shapes.

3. RESULTS AND DISCUSSION

3.1. Electrochemical Performance of the FeS_2−Ca Cell. The electrochemical performance of the Ca/FeS_2 cells was investigated with three electrolytes, 1.5 M $Ca(BH_4)_2$/THF, 1.5 M $Ca(BH_4)_2$ + 0.1 M $LiBH_4$/THF, and 0.5 M $Ca(BH_4)_2$ + 1.5 M $LiBH_4$/THF. As shown in Figure 1a and Figure S3, in the 1.5 M $Ca(BH_4)_2$/THF electrolyte without $LiBH_4$ addition, FeS_2 delivered almost no capacity. Adding 0.1 M $LiBH_4$ into the 1.5 M $Ca(BH_4)_2$/THF electrolyte could trigger the electrochemical process between the FeS_2 cathode and the Ca anode, which was demonstrated by the increased capacity and a discharge plateau at around 1.1 V. Nevertheless, the discharge capacity was still limited to 25 mAh g^{-1}, suggesting a poor electrochemical activity of the Ca/FeS_2 system. Further optimization of the electrolyte concentration to 0.5 M $Ca(BH_4)_2$ + 1.5 M $LiBH_4$/THF significantly enhanced the electrochemical performance (Figure 1b,c). The Ca/FeS_2 cell exhibited a flat discharge plateau at around 1.3 V, delivering a high initial discharge capacity of 809 mAh g^{-1}. This is close to the theoretical capacity of the conversion from Fe^{2+} to Fe^0 and S_2^{2-} to S^{2-} reported in Li-ion batteries,[20,21] proving the high electrochemical activity of the Ca/FeS_2 system after the addition of a sufficient amount of Li^+. In the first charge, the cell delivered a capacity of 496 mAh g^{-1}. The significant difference between the first discharge and charge capacities could imply that the electrochemical process of the FeS_2 in the first cycle is not reversible, which will be discussed later in this work. In the second cycle, the cell delivered a discharge capacity of 493 mAh g^{-1} with a Coulombic efficiency of 98.3%. The average discharge potential was between 1.4 and 1.6 V, which is lower than the theoretical potential calculated (Supporting Information, calculation of the theoretical potential). After 200 cycles, a high discharge capacity of 303 mAh g^{-1} with a Coulombic efficiency of 96.7% remained. The FeS_2−Ca cell with the 0.5 M $Ca(BH_4)_2$ + 1.5 M $LiBH_4$/THF electrolyte also exhibited an excellent rate performance (Figure 1d,e). It displayed discharge capacities of 474, 434, 375, and 317 mAh g^{-1} at C/8, C/5, C/2, and 1C, respectively. When the C-rate gradually reverted to C/8, the discharge capacity was restored to 399 mAh g^{-1}.

3.2. FeS_2 Cathode Reaction Mechanism. The addition of $LiBH_4$ vastly improved the discharge capacity of the FeS_2−Ca cell in initial cycles, which may be due to the following two reasons: (1) the kinetic of the Li^+ ion is superior to that of the Ca^{2+} ion, which is beneficial to the FeS_2 cathode reaction during charge/discharge, and (2) the $LiBH_4$ reduces the overpotential of the FeS_2−Ca cell significantly by decreasing

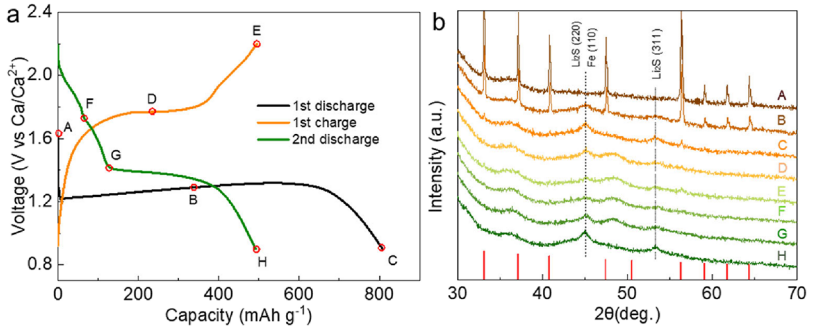

Figure 3. Voltage profiles of the FeS_2−Ca cell with the 0.5 M $Ca(BH_4)_2$ + 1.5 M $LiBH_4$/THF electrolyte (a) and the corresponding *ex situ* XRD measurements (b).

the Ca anode plating/stripping overpotential, which could also increase the discharge capacity of the cell. To clarify which of the two mentioned hypotheses is dominant, three-electrode cell measurements were conducted. As shown in Figure 2, the overpotentials of the Ca anodes (blue curves) were lower than 0.3 V in these three electrolytes, which influenced the voltage profiles of the Ca/FeS_2 full cell negligibly. Instead, the voltage profiles of the full cells were dominated by the FeS_2 cathode side. In the 1.5 M $Ca(BH_4)_2$/THF electrolyte (Figure 2a,b), the FeS_2 cathode scarcely reacted during discharge, leading to a fast voltage drop and ultralow capacity. The discharge capacity increased with the addition of $LiBH_4$ (Figure 2c−f), proving that the Li^+ ions were highly involved in the cathode discharge reaction. The three-electrode measurements proved that hypothesis 1, not hypothesis 2, is the reason for the high capacity of the FeS_2/Ca cell with 1.5 M $LiBH_4$ + 0.5 M $Ca(BH_4)_2$/THF in the initial cycles.

Ex situ XRD was used to clarify the cathode reaction mechanism in the 0.5 M $Ca(BH_4)_2$ + 1.5 M $LiBH_4$/THF electrolyte. As displayed in Figure 3, the FeS_2 peaks faded away during the first discharge, while two new broad peaks centered at 44.8 and 53.1° emerged. The signal at 44.8° can be indexed to Li_2S (220) and/or Fe (110).[25] Since these two features overlap, precise identification is difficult. The other one at 53.1° corresponds to the Li_2S (311). The intensity of these two features was weakened during the first charge. However, signals of FeS_2 could not be observed even at the end of the charge (EOC), suggesting that the reaction in the first discharge may not be reversible. Afterward, the results indicated a reversible reaction in the following discharge as the two characteristic peaks at 44.8 and 53.1° gained intensity again. Taken together, the e*x situ* XRD demonstrated that the FeS_2 was converted to Li_2S at the end of discharge, which could not be oxidized to FeS_2 in the following charge, leading to a significant irreversible capacity loss. After the first discharge, the conversion became reversible.

High-resolution transmission electron microscopy (HRTEM) was employed to further reveal the reaction mechanism of the FeS_2 cathode. As shown in Figure 4, the selected area electron diffraction (SAED) of the cathode material at the end of the first discharge (EOD) displayed vague diffraction rings, which could be assigned to Li_2S and/or Fe (Figure 4a). The lattice fringes of these two products were also captured in images with a higher magnification (Figure 4b), proving the conversion reaction from FeS_2 to Li_2S and Fe. Nevertheless, it is still unclear whether the CaS was formed or not, given that Ca^{2+} and Li^+ coexisted in the electrolyte and the d-spacing of CaS was similar to that of Li_2S (Figure S4). The

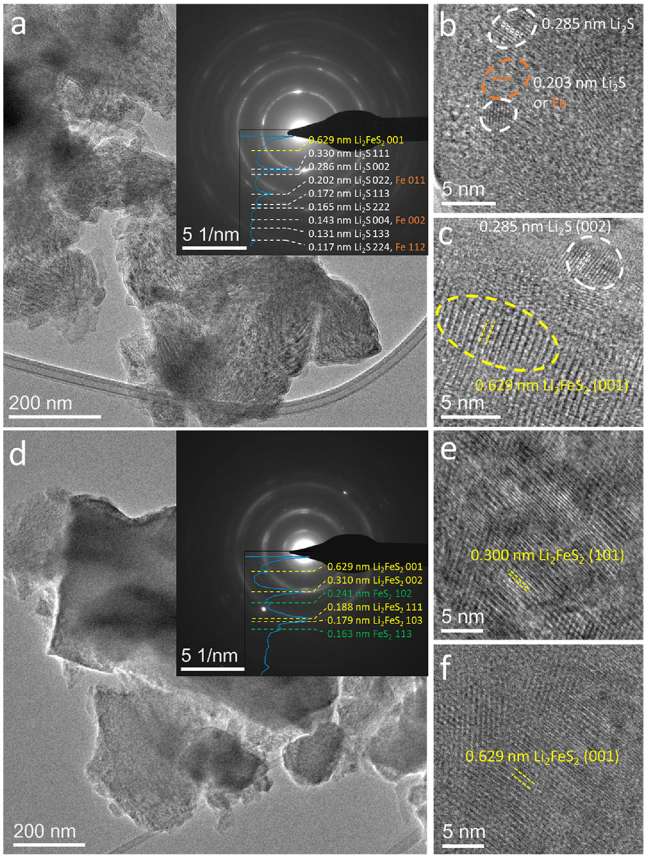

Figure 4. TEM images of the samples at (a−c) EOD and (d−f) EOC. Insets of a and d: corresponding SAED patterns.

elemental mapping of this sample is displayed in Figure S5. It demonstrated that the signals of sulfur and iron seem to be more or less evenly distributed across the whole nanoparticles. Calcium rather accumulates at the surface of the nanoparticles with a small atomic fraction of 5.1%, much lower than that of S (63.5%), implying that the calcium should be mainly from electrolyte residues. The HRTEM images and EDX results, combined with the three-electrode data in Figure 2, proved that Li^+ was the dominant ion to drive the conversion reaction rather than Ca^{2+}. Apart from Li_2S and Fe, the lattice fringes of Li_2FeS_2 were also seen in the HRTEM images of the discharged sample (Figure 4c). This was supposed to be the intermediate product from the FeS_2 reduction. Based on these results and previous reports, the reaction during charge and discharge is supposed to be the most widely accepted

mechanism (Supporting Information, reaction mechanism part).[21,26−28] Indeed, FeS_2 and Li_2FeS_2 became more substantial in the nanodomains at EOC (Figure 4d−f). No $FeS_{8/7}$ diffraction signal was detected, probably due to its low content.

The chemical state of FeS_2 cathodes in different charge/discharge states was also investigated in XPS measurements. Most importantly, the S 2p detail spectra provided more solid evidence for this conversion mechanism. As shown in Figure 5,

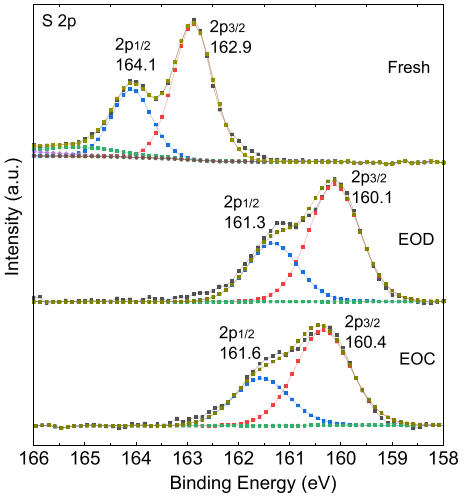

Figure 5. S 2p XPS spectra of FeS_2 cathodes at different charge/discharge states.

a peak doublet was detected in the spectrum of the pristine FeS_2 at 162.9 and 164.1 eV, which can be assigned to the S_2^{2-} of FeS_2.[29−31] The peak doublet shifted to the lower binding energy of 160.1 and 161.3 eV at EOD, indicating the conversion from S_2^{2-} to Li_2S.[32,33] After recharging the cell to 2.2 V (EOC), the binding energy did not recover to the pristine state. Instead, the negligible binding energy change between EOD and EOC proved that most of the sulfur species were preserved as S^{2-}, consistent with HRTEM analysis.

3.3. Beneficial Effect of $LiBH_4$ on the Ca Anode. After elucidating the reactions at the FeS_2 cathode and demonstrating the crucial role that Li^+ ions play here, we now turn to the Ca anode. Another impressive feature of the Ca/FeS_2 cell is its long cycle life, which indicates efficient Ca stripping/plating over long cycling. Concerning this, we evaluated the feasibility of the reversible Ca stripping/plating by galvanostatically cycling Ca/Ca symmetric cells in the three electrolytes (1.5 M $Ca(BH_4)_2$/THF, 1.5 M $Ca(BH_4)_2$ + 0.1 M $LiBH_4$/THF, and 0.5 M $Ca(BH_4)_2$ + 1.5 M $LiBH_4$/THF). As shown in Figure 6a,b, all three electrolytes exhibited moderate Ca plating/stripping overpotentials below 0.1 V over the first 20 h (except for the first activation cycle). Afterward, however, the voltage value of 1.5 M $Ca(BH_4)_2$/THF increased terribly, followed by severe fluctuations after 40 h, indicating a poor plating/stripping process. In sharp contrast, outstanding plating/stripping performance could be achieved in the electrolytes containing $LiBH_4$. The 1.5 M $Ca(BH_4)_2$ + 0.1 M $LiBH_4$/THF electrolyte delivered a plating/stripping overpotential lower than 0.1 V over 150 h. Remarkably, the 0.5 M $Ca(BH_4)_2$ + 1.5 M $LiBH_4$/THF electrolyte underwent over 200 h of charge/discharge cycles with low overpotential, which decreased gradually from 101 to 34 mV over the initial 70 h and then maintained constant over 200 h. It has been reported that the addition of 0.4 M $LiBH_4$ into the 0.4 M $Ca(BH_4)_2$/THF electrolyte could promote the plating/stripping reversibility of the Ca metal anode due to the enhanced desolvation kinetics of Ca^{2+} ions in the electrolyte,[10] which is also supposed to be

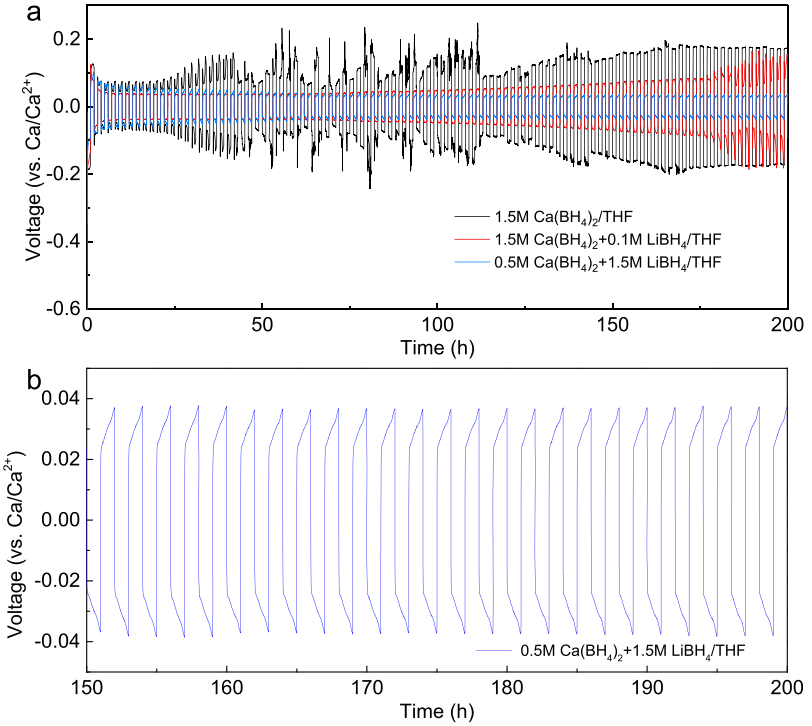

Figure 6. (a) Ca plating/stripping performance of Ca/Ca symmetric cells with different electrolytes under a current density of 0.1 mA cm^{-2} for 1 h at each step. (b) Magnification of (a) after 150 h.

the determining factor for the superior performance of our 0.5 M $Ca(BH_4)_2$ + 1.5 M $LiBH_4$/THF electrolyte. To clarify whether the positive effect of the presence of $LiBH_4$ comes from the desolvation energy or the passive film formation, the XPS measurement of Ca electrodes after plating Ca under a current density of 0.1 mA cm^{-2} was conducted, and the results are shown in Figure S6. The Ca 2p spectra with two peaks centered at 346.5 (Ca 2p1/2) and 350.0 (Ca 2p3/2) eV could be assigned to $CaCO_3$, suggesting that the $CaCO_3$ may be one of the components of the passivation layer. In the C1s spectra, three peaks centered at 284.8, 286.3, and 288.4 eV were assigned to C=C, C−O, and C=O bonds. These compounds may originate from THF decomposition or the adsorbents. The O 1s spectrum could be fitted into two peaks at 530.8 (C=O) and 532.5 (C−O) eV, which is in good agreement with the C spectrum.[34] No significant difference could be observed from the XPS spectra of these two electrode surfaces, indicating that the interfacial compositions or the passivation layers on the Ca electrodes are similar. This result is consistent with the previous report.[10] After Ca deposition, no XPS peak of Li could be detected on the electrode surface in the 0.5 M $Ca(BH_4)_2$ + 1.5 M $LiBH_4$/THF electrolyte, proving the lithium rather than calcium deposited on the anode during the electrochemical process under 0.1 mA cm^{-2}. The XRD pattern of the deposit on the Au working electrode was also recorded (Figure S7) to investigate the composition of the deposits. The Ca signals could be indexed, and no Li peak was observed, which is consistent with XPS data. It should be noted that we got this conclusion based on a current density of 0.1 mA cm^{-2}. The deposition behavior of this electrolyte under high current density may be different, given that higher current densities favor Li co-deposition for kinetic and mass transport reasons, which is currently under study. SEM and EDS analysis (Figure S8) shows that the deposited calcium takes on a round flower-like shape. The absence of dendritic calcium could reduce the possibility of penetrating through the separator and avoid a short circuit. However, it should be noted that the sample was exposed to air for a short time during being transferred to the SEM instrument. Calcium could react with oxygen during this period of time. That is why a certain amount of oxygen was also detected.

4. CONCLUSIONS

In summary, we report an attractive Ca battery with high capacity and long cycle life, composed of a conversion-type FeS_2 cathode and a metallic Ca metal anode. It combined the virtues of the remarkable capacity of FeS_2 and the ready availability of Ca due to its high abundance in the earth's crust. The $Ca(BH_4)_2$ + $LiBH_4$/THF hybrid electrolyte ensured the kinetically favorable Li-driven conversion of FeS_2, thus bypassing the sluggish Ca^{2+} ion diffusion in the cathode lattice. Simultaneously, it enhanced the desolvation kinetics of Ca^{2+} ions, resulting in excellent reversibility with a small overpotential at the Ca anode over long-term cycling. Consequently, the FeS_2−Ca battery exhibited a high discharge capacity of 303 mAh g^{-1} with a Coulombic efficiency of 96.7% over 200 cycles, which is superior to other batteries using a dual-salt electrolyte and a calcium metal anode (Table S1). Compared with some other conversion cathode/Ca cells,[5,7] our concept could achieve long cycle life with commercially available salt easily. Further investigation about this concept will focus on how to reduce the electrolyte/Li^+ amount to make it more practical.

■ ASSOCIATED CONTENT

● Supporting Information

The Supporting Information is available free of charge at https://pubs.acs.org/doi/10.1021/acsami.2c11337.

SEM, EDS, measurements of FeS_2 materials, electrochemical performance, lattice parameter of Fe, Li_2S, CaS, and Li_2FeS_2, and XRD of Ca depositions (PDF)

■ AUTHOR INFORMATION

Corresponding Authors

Zhen Meng − *Helmholtz Institute Ulm (HIU) Electrochemical Energy Storage, Ulm D-89081 Baden-Württemberg, Germany*; orcid.org/0000-0001-5756-9159; Email: zhen.meng@partner.kit.edu

Zhirong Zhao-Karger − *Helmholtz Institute Ulm (HIU) Electrochemical Energy Storage, Ulm D-89081 Baden-Württemberg, Germany*; orcid.org/0000-0002-7233-9818; Email: zhirong.zhao-karger@kit.edu

Authors

Adam Reupert − *Helmholtz Institute Ulm (HIU) Electrochemical Energy Storage, Ulm D-89081 Baden-Württemberg, Germany*

Yushu Tang − *Institute of Nanotechnology, Karlsruhe Institute of Technology (KIT), Eggenstein-Leopoldshafen D-76344 Baden-Württemberg, Germany*

Zhenyou Li − *Helmholtz Institute Ulm (HIU) Electrochemical Energy Storage, Ulm D-89081 Baden-Württemberg, Germany*; orcid.org/0000-0001-9624-2124

Guruprakash Karkera − *Helmholtz Institute Ulm (HIU) Electrochemical Energy Storage, Ulm D-89081 Baden-Württemberg, Germany*

Liping Wang − *Helmholtz Institute Ulm (HIU) Electrochemical Energy Storage, Ulm D-89081 Baden-Württemberg, Germany*; orcid.org/0000-0002-4113-2208

Ananyo Roy − *Helmholtz Institute Ulm (HIU) Electrochemical Energy Storage, Ulm D-89081 Baden-Württemberg, Germany*

Thomas Diemant − *Helmholtz Institute Ulm (HIU) Electrochemical Energy Storage, Ulm D-89081 Baden-Württemberg, Germany*

Maximilian Fichtner − *Helmholtz Institute Ulm (HIU) Electrochemical Energy Storage, Ulm D-89081 Baden-Württemberg, Germany; Institute of Nanotechnology, Karlsruhe Institute of Technology (KIT), Eggenstein-Leopoldshafen D-76344 Baden-Württemberg, Germany*; orcid.org/0000-0002-7127-1823

Complete contact information is available at: https://pubs.acs.org/10.1021/acsami.2c11337

Notes

The authors declare no competing financial interest.

■ ACKNOWLEDGMENTS

This work contributes to the research performed at CELEST (Center for Electrochemical Energy Storage Ulm-Karlsruhe) and was funded by the German Research Foundation (DFG) under Project ID 390874152 (POLiS Cluster of Excellence). Electron microscopy was supported by the Karlsruhe Nano Micro Facility (KNMF; www.knmf.kit.edu), a Helmholtz

Research Infrastructure at Karlsruhe Institute of Technology (KIT; www.kit.edu).

REFERENCES

(1) Ponrouch, A.; Frontera, C.; Bardé, F.; Palacán, M. R. Towards a Calcium-Based Rechargeable Battery. *Nat. Mater.* **2016**, *15*, 169−172.

(2) Li, Z.; Fuhr, O.; Fichtner, M.; Zhao-Karger, Z. Towards Stable and Efficient Electrolytes for Room-Temperature Rechargeable Calcium Batteries. *Energy Environ. Sci.* **2019**, *12*, 3496−3501.

(3) Shyamsunder, A.; Blanc, L. E.; Assoud, A.; Nazar, L. F. Reversible Calcium Plating and Stripping at Room Temperature Using a Borate Salt. *ACS Energy Lett.* **2019**, *4*, 2271−2276.

(4) Rong, Z.; Malik, R.; Canepa, P.; Sai Gautam, G.; Liu, M.; Jain, A.; Persson, K.; Ceder, G. Materials Design Rules for Multivalent Ion Mobility in Intercalation Structures. *Chem. Mater.* **2015**, *27*, 6016−6021.

(5) Li, Z.; Vinayan, B. P.; Diemant, T.; Behm, R. J.; Fichtner, M.; Zhao-Karger, Z. Rechargeable Calcium−Sulfur Batteries Enabled by an Efficient Borate-Based Electrolyte. *Small* **2020**, *16*, 2001806.

(6) Bitenc, J.; Scafuri, A.; Pirnat, K.; Lozinšek, M.; Jerman, I.; Grdadolnik, J.; Fraisse, B.; Berthelot, R.; Stievano, L.; Dominko, R. Electrochemical Performance and Mechanism of Calcium Metal-Organic Battery. *Batteries Supercaps* **2021**, *4*, 214−220.

(7) Scafuri, A.; Berthelot, R.; Pirnat, K.; Vizintin, A.; Bitenc, J.; Aquilanti, G.; Foix, D.; Dedryvère, R.; Arčon, I.; Dominko, R.; et al. Spectroscopic Insights into the Electrochemical Mechanism of Rechargeable Calcium/Sulfur Batteries. *Chem. Mater.* **2020**, *32*, 8266−8275.

(8) Tang, K.; Du, A.; Dong, S.; Cui, Z.; Liu, X.; Lu, C.; Zhao, J.; Zhou, X.; Cui, G. A Stable Solid Electrolyte Interphase for Magnesium Metal Anode Evolved from a Bulky Anion Lithium Salt. *Adv. Mater.* **2020**, *32*, 1904987.

(9) Song, H.; Su, J.; Wang, C. Hybrid Solid Electrolyte Interphases Enabled Ultralong Life Ca-Metal Batteries Working at Room Temperature. *Adv. Mater.* **2021**, *33*, 2006141.

(10) Jie, Y.; Tan, Y.; Li, L.; Han, Y.; Xu, S.; Zhao, Z.; Cao, R.; Ren, X.; Huang, F.; Lei, Z.; et al. Electrolyte Solvation Manipulation Enables Unprecedented Room-Temperature Calcium-Metal Batteries. *Angew. Chem., Int. Ed.* **2020**, *59*, 12689−12693.

(11) Cheng, Y.; Shao, Y.; Zhang, J.-G.; Sprenkle, V. L.; Liu, J.; Li, G. High Performance Batteries Based on Hybrid Magnesium and Lithium Chemistry. *Chem. Commun.* **2014**, *50*, 9644−9646.

(12) Yagi, S.; Ichitsubo, T.; Shirai, Y.; Yanai, S.; Doi, T.; Murase, K.; Matsubara, E. A Concept of Dual-Salt Polyvalent-Metal Storage Battery. *J. Mater. Chem. A* **2014**, *2*, 1144−1149.

(13) Cho, J.-H.; Aykol, M.; Kim, S.; Ha, J.-H.; Wolverton, C.; Chung, K. Y.; Kim, K.-B.; Cho, B.-W. Controlling the Intercalation Chemistry to Design High-Performance Dual-Salt Hybrid Rechargeable Batteries. *J. Am. Chem. Soc.* **2014**, *136*, 16116−16119.

(14) Gao, T.; Han, F.; Zhu, Y.; Suo, L.; Luo, C.; Xu, K.; Wang, C. Hybrid Mg2+/Li+ Battery with Long Cycle Life and High Rate Capability. *Adv. Energy Mater.* **2015**, *5*, 1401507.

(15) Yoo, H. D.; Liang, Y.; Li, Y.; Yao, Y. High Areal Capacity Hybrid Magnesium−Lithium-Ion Battery with 99.9% Coulombic Efficiency for Large-Scale Energy Storage. *ACS Appl. Mater. Interfaces* **2015**, *7*, 7001−7007.

(16) Su, S.; Huang, Z.; NuLi, Y.; Tuerxun, F.; Yang, J.; Wang, J. A Novel Rechargeable Battery with a Magnesium Anode, a Titanium Dioxide Cathode, and a Magnesium Borohydride/Tetraglyme Electrolyte. *Chem. Commun.* **2015**, *51*, 2641−2644.

(17) Gao, T.; Noked, M.; Pearse, A. J.; Gillette, E.; Fan, X.; Zhu, Y.; Luo, C.; Suo, L.; Schroeder, M. A.; Xu, K.; et al. Enhancing the Reversibility of Mg/S Battery Chemistry through Li^+ Mediation. *J. Am. Chem. Soc.* **2015**, *137*, 12388−12393.

(18) Yu, X.; Boyer, M. J.; Hwang, G. S.; Manthiram, A. Toward a Reversible Calcium-Sulfur Battery with a Lithium-Ion Mediation Approach. *Adv. Energy Mater.* **2019**, *9*, 1803794.

(19) Zhang, Y.; Xie, J.; Han, Y.; Li, C. Dual-Salt Mg-Based Batteries with Conversion Cathodes. *Adv. Funct. Mater.* **2015**, *25*, 7300−7308.

(20) Liu, J.; Wen, Y.; Wang, Y.; van Aken, P. A.; Maier, J.; Yu, Y. Carbon-Encapsulated Pyrite as Stable and Earth-Abundant High Energy Cathode Material for Rechargeable Lithium Batteries. *Adv. Mater.* **2014**, *26*, 6025−6030.

(21) Zhu, Y.; Fan, X.; Suo, L.; Luo, C.; Gao, T.; Wang, C. Electrospun FeS_2@Carbon Fiber Electrode as a High Energy Density Cathode for Rechargeable Lithium Batteries. *ACS Nano* **2016**, *10*, 1529−1538.

(22) Zhang, K.; Park, M.; Zhou, L.; Lee, G.-H.; Shin, J.; Hu, Z.; Chou, S.-L.; Chen, J.; Kang, Y.-M. Cobalt-Doped FeS_2 Nanospheres with Complete Solid Solubility as a High-Performance Anode Material for Sodium-Ion Batteries. *Angew. Chem., Int. Ed.* **2016**, *55*, 12822−12826.

(23) Wan, Y.; Song, K.; Chen, W.; Qin, C.; Zhang, X.; Zhang, J.; Dai, H.; Hu, Z.; Yan, P.; Liu, C.; et al. Ultra-High Initial Coulombic Efficiency Induced by Interface Engineering Enables Rapid, Stable Sodium Storage. *Angew. Chem., Int. Ed.* **2021**, *60*, 11481−11486.

(24) Xu, X.; Cai, T.; Meng, Z.; Ying, H.; Xie, Y.; Zhu, X.; Han, W.-Q. FeS_2 Nanocrystals Prepared in Hierarchical Porous Carbon for Lithium-Ion Battery. *J. Power Sources* **2016**, *331*, 366−372.

(25) Zou, J.; Zhao, J.; Wang, B.; Chen, S.; Chen, P.; Ran, Q.; Li, L.; Wang, X.; Yao, J.; Li, H.; et al. Unraveling the Reaction Mechanism of FeS_2 as a Li-Ion Battery Cathode. *ACS Appl. Mater. Interfaces* **2020**, *12*, 44850−44857.

(26) Iwakura, C.; Isobe, N.; Tamura, H. Initial Open Circuit Voltages and Discharge Reaction Mechanisms in Non-Aqueous Electrolyte Li/FeS_2 Cells. *Electrochim. Acta* **1983**, *28*, 277−283.

(27) Yersak, T. A.; Macpherson, H. A.; Kim, S. C.; Le, V.-D.; Kang, C. S.; Son, S.-B.; Kim, Y.-H.; Trevey, J. E.; Oh, K. H.; Stoldt, C.; et al. Solid State Enabled Reversible Four Electron Storage. *Adv. Energy Mater.* **2013**, *3*, 120−127.

(28) Fong, R.; Dahn, J. R.; Jones, C. H. W. Electrochemistry of Pyrite-Based Cathodes for Ambient Temperature Lithium Batteries. *J. Electrochem. Soc.* **1989**, *136*, 3206−3210.

(29) Guo, Y.; Shang, C.; Zhang, X.; Wang, E. Electrocatalytic Hydrogen Evolution Using the MS_2@MoS_2/RGO (M = Fe or Ni) Hybrid Catalyst. *Chem. Commun.* **2016**, *52*, 11795−11798.

(30) Yin, J.; Li, Y.; Lv, F.; Lu, M.; Sun, K.; Wang, W.; Wang, L.; Cheng, F.; Li, Y.; Xi, P.; et al. Oxygen Vacancies Dominated NiS_2/CoS_2 Interface Porous Nanowires for Portable Zn−Air Batteries Driven Water Splitting Devices. *Adv. Mater.* **2017**, *29*, 1704681.

(31) Qiu, X.; Liu, M.; Hayashi, T.; Miyauchi, M.; Hashimoto, K. Solution-Based Synthesis of Pyrite Films with Enhanced Photocurrent Generation. *Chem. Commun.* **2013**, *49*, 1232−1234.

(32) Liang, X.; Hart, C.; Pang, Q.; Garsuch, A.; Weiss, T.; Nazar, L. F. A Highly Efficient Polysulfide Mediator for Lithium−sulfur Batteries. *Nat. Commun.* **2015**, *6*, 5682.

(33) Helen, M.; Reddy, M. A.; Diemant, T.; Golla-Schindler, U.; Behm, R. J.; Kaiser, U.; Fichtner, M. Single Step Transformation of Sulphur to Li_2S_2/Li_2S in Li-S Batteries. *Sci. Rep.* **2015**, *5*, 12146.

(34) Moulder, J. F.; Stickle, W. F.; Sobol, P. E.; Bomben, K. D. Handbook of X-Ray Photoelectron Spectroscopy. *Physical Electronics*; CiNii, 1995.